Evolution of flow around a finite circular cylinder in the critical transition range

Jiun-Jih Miau*, Yng-Ru Chen and Yu-Hsiang Chen

National Cheng Kung University, Tainan, Taiwan 70101

* Correspondent author: jjmiau@mail.ncku.edu.tw

Abstract

Experimental results obtained in two wind tunnels on flow over a finite cylinder of L/D =4 in the critical transition range are reported. Based on the drag and lift force measurements, the critical and super-critical ranges can be distinguished into four sub-ranges, which bear a similarity to those reported on flow over a two-dimensional circular cylinder. However, oil-film visualization made in the critical transition range indicates that the footprint of the horse shoe vortex in the base region gets more significant as Reynolds number increased. On-set of the transition is found to initiate in the base region, learned from a comparison of the real-time pressure signals measured at three height levels of the model.

Keyword: *finite circular cylinder, critical transition, wind-tunnel experiment, horse shoe vortex*

1. Introduction

More than one century ago, Wieselsberger [1] reported on the critical transition phenomenon for a finite circular cylinder of L/D =5, where L and D denote the length and diameter of the model respectively. The drag coefficient dropped drastically within a narrow range of Reynolds numbers of 10^5, like the case of flow over a two-dimensional circular cylinder. The phenomenon is known for the drag crisis, featuring the formation of laminar separation bubbles named LSB on the model surface that alters the aerodynamic flow dramatically.

In the literature, studies on the critical transition phenomenon for a finite circular cylinder are comparatively less than those for a two-dimensional circular cylinder, for which there are three sub-regimes identified, namely, the sub-critical, one-bubble and two bubble states [2]. On the other hand, extensive studies were made at sub-critical Reynolds numbers. It is noteworthy that for aspect ratio less than 4 [3], the vortex shedding phenomenon is switched from anti-symmetric (Karman type) to symmetric (arch type) vortex shedding.

This paper is focused on the evolution of flow around a finite circular cylinder of the aspect ratio 4. The results reported are based on a series of experiment work conducted in two wind tunnels, from which the quality of the experimental data is validated.

2. Experimental methods

Experiments were carried out in two wind tunnels. One named Wind Tunnel A has a test section of 3m by 4m in cross section, in which the freestream velocity can reach 30 m/s and the turbulence intensity measured at 10 and 20 m/s is about 0.35 %. [4] The other named Wind Tunnel B has a test section of 1 m by 1 m in cross section, in which the freestream velocity can reach 40 m/s and the turbulence intensity measured is about 0.7 %. [5]

Two finite circular cylinder models made of acrylic, whose surface roughness was less than $1\text{x}10^{-6}$ m, were employed. [6] Their diameters named D were 300 mm and 150 mm for the experiments conducted in Wind Tunnels A and B, respectively. In terms of the relative roughness based on D, both are less than $1\text{x}10^{-5}$, therefore are regarded as the smooth circular cylinder models as far as the critical transition phenomenon is concerned. [7] Concerning the blockage ratios of the two models in Wind Tunnels A and B, they are 3% and 9%, respectively.

In Wind Tunnel A, the model was situated 2.8 m downstream of the inlet of the test section on the floor, where the boundary layer thickness measured was about 0.06 m. In Wind Tunnel B, the model was situated at 3.4 m downstream of the inlet of the test section, where the boundary layer thicknesses on the top and bottom walls measured were 0.18 m and 0.1 m, respectively. [8]

Pressure measurements were made in both of Wind Tunnels A and B. Locations of the pressure taps on an experimental model are indicated in Fig. 1, with a coordinate system defined that x, y and z denote the streamwise, lateral and vertical directions, respectively. In addition, $\theta = 0°$ is the angular location corresponding to the forward stagnation point of the model. In Wind Tunnel A, the model was situated on the floor of the test section; in Wind Tunnel B, the model could be mounted on either of the top or bottom wall of the test section.

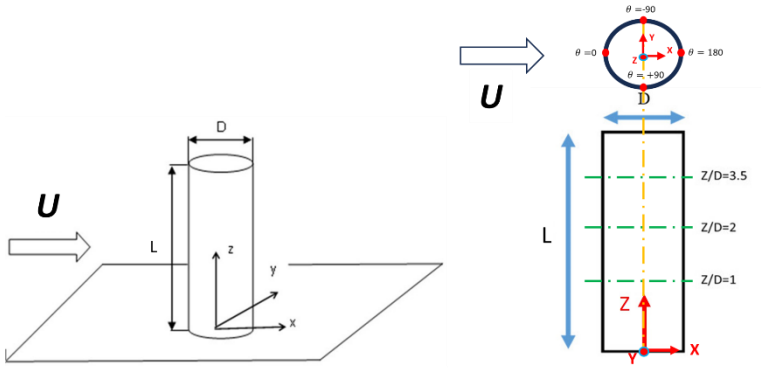

Fig. 1 Schematics of the finite circular cylinder model and the coordinate system employed. [6]

Force measurements of the model were made in Wind Tunnel B using a two-component balance situated above the test section. [9] The model was mounted on the top wall. In this case, pressure measurements were made together with force measurements.

Oil-film visualization was conducted in Wind Tunnel B for the model situated on the floor of the test section. [10] The oil film was prepared by mixing paraffin oil, silicone oil, oleic acid and TiO_2.

Reynolds number Re is defined in (1), based on U and D. U denotes the free stream velocity measured at the inlet of the test section; ν denotes the kinematic viscosity of the air in wind tunnel.

$$Re = \frac{UD}{\nu} \qquad (1)$$

Drag and lift coefficients denoted as C_D and C_L, respectively, are defined as follows.

$$C_D = \frac{F_D}{\frac{1}{2}\rho_{air} U^2 A_C} \qquad (2)$$

$$C_L = \frac{F_L}{\frac{1}{2}\rho_{air} U^2 A_C} \qquad (3)$$

F_D and F_L denote the instantaneous drag and lift forces measured, respectively; ρ_{air} denotes the density of air under the flow condition; A_C denotes the cross-sectional area of the model facing the free stream, which is equal to LD. $\overline{C_D}$ and $\overline{C_L}$ denote the time-averaged drag and lift coefficients respectively, which were reduced from a set of force measurement over 120 sec.

The pressure coefficient C_P reduced from the real-time pressure measurement at a pressure tap is expressed below.

$$C_P = \frac{P - P_{static}}{\frac{1}{2}\rho_{air} U^2} \qquad (4)$$

In (4), P denotes the instantaneous pressure measured at a pressure tap, P_{static} denotes the time-averaged free stream pressure measured by the Pitot tube situated at the inlet of the test section. In addition, the time-averaged pressure coefficient reduced from a set of measurements over 120 sec is denoted as $\overline{C_P}$.

3. Results and discussion

3.1 The critical transition ranges identified in Wind Tunnels A and B

Figure 2 compares the distributions of $\overline{C_{Pb}}$ of two models at z/D=1, 2 and 3.5 obtained in Wind Tunnels A and B, where $\overline{C_{Pb}}$ denotes the $\overline{C_P}$ value measured at $\theta = 180°$. The data are reproduced from Tsai [6]. Essentially, the ranges of the critical transition seen in the two wind tunnels are in good agreement, and are comparable to that seen in the $\overline{C_D}$ curve of a finite circular cylinder model of the aspect ratio 5 [1]. Nevertheless, with a close look on the figure, discrepancies are noted and pointed out below. In Wind Tunnel A, the transition takes place between Re= 3.3 x10^5 to 3.9 x10^5, whereas in Wind Tunnel B the transition takes place in a narrower range between Re= 3.5x10^5 to 3.8x10^5. The difference could be reasoned due to a number of factors, including the ratio of the boundary layer thicknesses on the ground plate to D, the blockage ratios of the models, the flow characteristics of the wind tunnels and roughness of the models despite that they

both fall in the category of smooth model. However, no further investigations concerning these factors were made in this study.

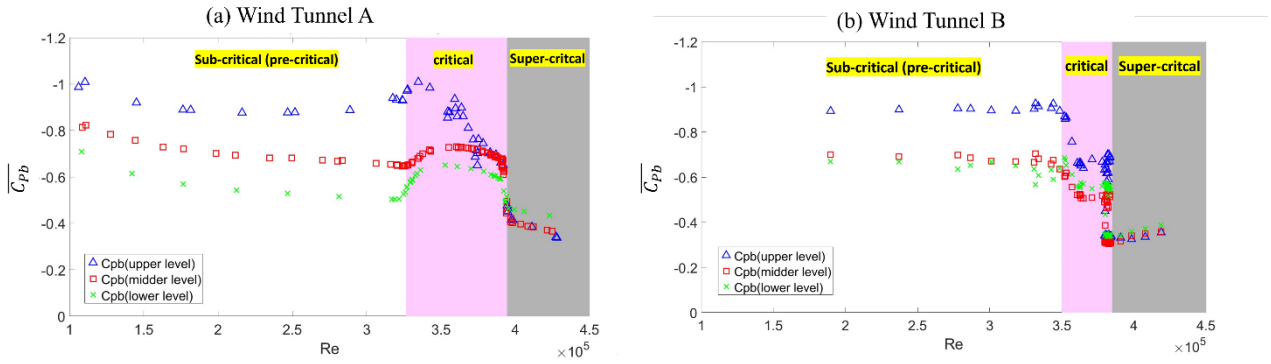

Fig. 2 Variations of $\overline{C_{Pb}}$ at z/D=1, 2 and 3.5 with *Re* obtained in (a) Wind Tunnel A and (b) Wind Tunnel B. [6]

At pre-critical *Re*, say Re= 2 x10^5 to 2.5x10^5, the $\overline{C_{Pb}}$ values at z/*D*= 3.5, where is near the free end of the model, are about -1, considerably lower than those at z/*D*= 2 and 1. This is attributed to the downwash motion from the free end of the model. [11] Towards the super-critical range, the $\overline{C_{Pb}}$ values at the three height levels are converged to a less negative value about -0.4. Thus, one can say that in the super-critical range, the effect due to the formation of LSBs to the pressure distribution of the model outweighs the downwash motion from the free end of the model.

Figure 3 shows the variations of the cross-correlation coefficients of C_P at $\theta = \pm 90°$ with *Re*, for z/*D*=1, 2 and 3.5, in Wind Tunnel A. The data are reproduced from Tsai [6]. Two interesting features are noted. Firstly, at pre-critical *Re*, say, 2x10^5 to 2.5x10^5, the cross-correlation coefficients stay positive; the higher the z/*D*, the higher the values close to 1. This is reasoned that for the present model of the aspect ratio 4, the arch-type vortex shedding is prevailing around the model. [3, 12] At lower z/*D*, the horse-shoe vortex in the base region comes into play to interact with the arch-type vortex shedding, which has an impact to the cross correlation. Secondly, in the critical transition range, the differences between the variations of the cross-coefficients at z/*D*=1, 2 and 3.5 are remarkable. In viewing that the pressure fluctuations measured in the critical transition range are dominated by unsteady formation of separation bubbles, the differences noted among z/*D*=1, 2 and 3.5 can be further explained below. At z/*D* =3.5 the situation featuring unsteady, asymmetric bubble formation is pronounced throughout the critical transition range. At z/*D* = 2 and 1, this situation is comparatively less outstanding. Above observations suggest that the horse shoe vortex in the base region could play a significant role to damp the unsteadiness of bubble formation.

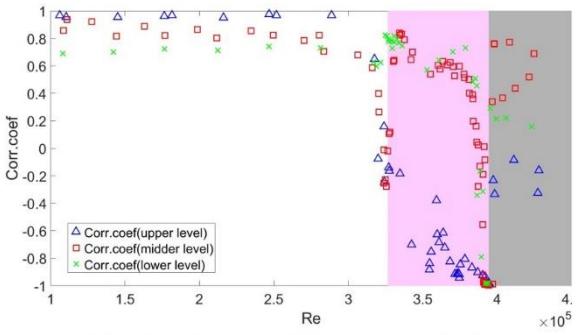

Fig. 3 Variations of the cross-correlation coefficients of C_P at $\theta = \pm 90°$, z/*D*=1, 2 and 3.5, with *Re* obtained in Wind Tunnel A. [6]

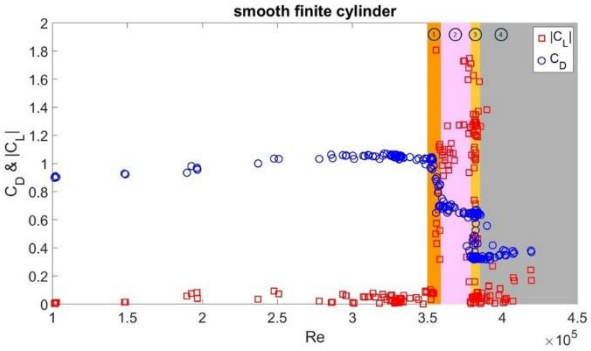

Fig. 4 Variations of $\overline{C_D}$ and $|\overline{C_L}|$ with *Re* reduced from the force measurements in Wind Tunnel B. [6]

3.2 Results of force measurements made in Wind Tunnel B

Figure 4 presents the time-averaged drag and lift coefficients of the model reduced from the force measurements obtained in Wind Tunnel B. The data are reproduced from Tsai [6]. Indicated in the figure is that the critical transition takes place in a range of *Re*=3.5x10^4 to 3.8x10^5, which is coincided with that seen in the $\overline{C_{Pb}}$ distributions in Fig. 2. In the range, $\overline{C_D}$ decreased from 1.2 to 0.4, while $\overline{C_L}$ in the absolute value, $|\overline{C_L}|$, reached a maximum of 1.8. The data shown in the critical and super-critical ranges can be further distinguished into four sub-ranges indicated in the figure, which bear a similarity to flow over a two-dimensional circular cylinder. [13, 14] Specifically, Sub-range 1 is referred to the transition from the pre-critical to one-bubble states; Sub-range 2 is referred to the one-bubble state; Subrange 3 is referred to the transition from one-bubble to two-bubble states; Sub-range 4 is referred to the two-bubble state. As noted, the $|\overline{C_L}|$ values appear remarkably high in the sub-ranges 1 and 3, in which the formation of separation bubbles are highly unsteady.

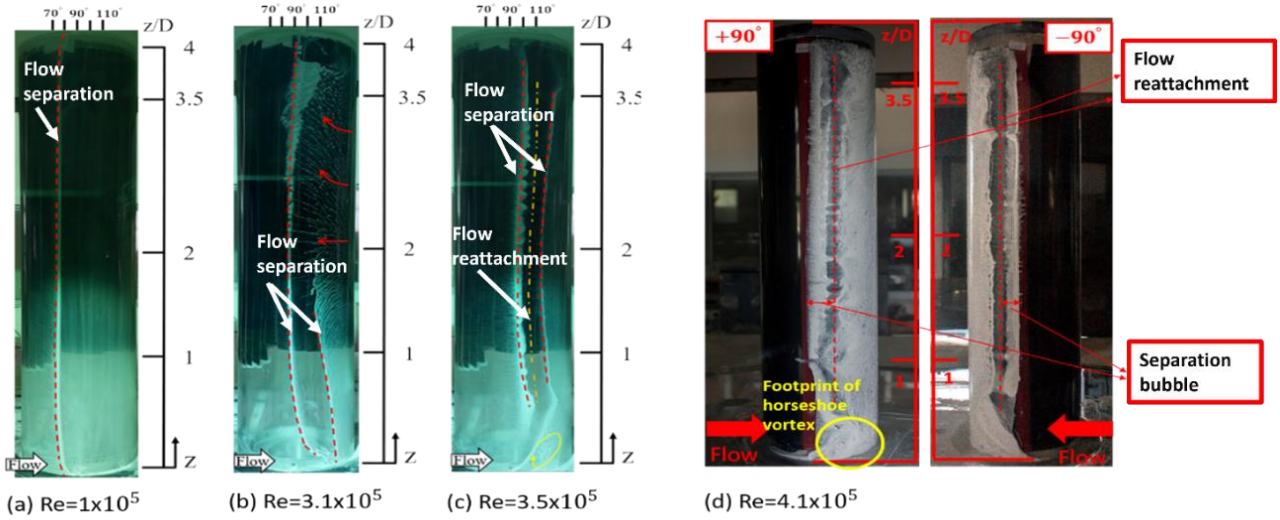

Fig. 5 Oil-film visualization images obtained at *Re*: (a) 1x10^5, (b) 3.1x10^5, (c) 3.5x10^5, and (d) 4.1x10^5. [15, 8]

3.3 Results of flow visualization made in Wind Tunnel B

Physical insights into the complex flow characteristics in the critical transition range can be gained with the oil-film visualization method. In Fig. 5, the photo images obtained at *Re*=1, 3.1, 3.5 and 4.1x10^5 are presented for discussion. The images of *Re*=1, 3.1 and 3.5x10^5 are reproduced from Zhuang [15]; the images of *Re*=4.1x10^5 are reproduced from Wu [8].

The image of Re=1x10^5 shows a typical pattern in the sub-critical regime that a separation line is formed at θ = 80°. The separation line appears two-dimensional, aligned in the spanwise direction from the free end to the base region.

The images of Re=3.1x10^{5}and 3.5x10^5 highlight the three-dimensional and intermittent nature of the flow in the critical transition range. The image of Re=3.1x10^5 represents a snapshot of flow near the model surface. In the region of z/*D*>2, flow appeared in deceleration that only one flow separation line was formed about θ = 90°, downstream of which massive reversed flow took place. On the other hand, in the region of z/*D*<2, the flow appeared rather not in deceleration. Two separation lines took place at θ = 90° and 110°-120°, respectively, inferring a LSB formed between the two separation lines. It is noteworthy that the flow appearances under these flow conditions were highly intermittent.

The image of Re=3.5x10^5 shows that away from the free end and base regions a LSB is formed between the two separation lines at θ = 100° and 120°. In the base region, a footprint of the horse shoe vortex downstream of θ=120° can be discerned.

Two images of Re=4.1x10^5 obtained on the two sides of the model depict the super-critical situation that LSBs were formed stably on the two sides, and the footprint of the horse vortex is remarkable. Flow reattachment regions on the two sides indicated by little oil-film remained appear rather three-dimensional, inferring that the LSBs are cellular like along the spanwise direction. [16]

Additional remark on the photo image of *Re*=3.1x10^5 is made here. The image clearly indicates that the state of the flow falls in the critical transition range. However, Figs. 2 and 4, which are concerned with the time-averaged flow properties mainly, show no indication in this regard. Therefore, the critical transition range should be scrutinized in a more careful manner.

3.4 An investigation into the on-set of the critical transition

Figure 6 compares the real-time C_P traces obtained at z/D=1, 2 and 3.5, $\theta = \pm 90°$, for Re= 2.11x10^5 to highlight a situation at the initialization of the critical transition. The C_P traces in this figure are reproduced from Zhuang [15]. In the figure, it is seen that more pronounced fluctuations are seen in the C_P traces at z/D=1, $\theta = \pm 90°$, in comparison with those at z/D=2 and 3.5. Moreover, in probing into the characteristic events of the fluctuations [17], it is further found that the time scale of the fluctuations is coincided with that of the arch-type vortex shedding, which is prevailing around the model under the flow condition. As a speculation, the on-set transition would be involved with an interaction between the horse shoe vortex in the base region and the arch-type vortex shedding. [18]

As Re increased, pronounced fluctuations get more visible in the C_P traces at z/D=2 and 3.5, $\theta = \pm 90°$. This trend can be realized in Fig. 7, in which variations of the skewness of the C_P traces with Re over the critical transition range are presented. The data are reproduced from Zhuang [15]. For Re in the range of 2x10^5 to 2.5x10^5, where the on-set of transition takes place in the base region, the skewness values at z/D=1, $\theta = \pm 90°$, show highly negative, less than -2, which appear the lowest among those of the three level heights measured. Plausibly, the remarkably negative is contributed by the pronounced fluctuations in the real-time trace seen in Fig. 6. The skewness values at z/D=2 gets decreased with Re to Re= 3.0x10^5 as indicated. At z/D=3.5 the skewness values stay about zero until Re= 3.2x10^5, where an abrupt drop to less than -2 is occurred, signifying that the critical transition sets in.

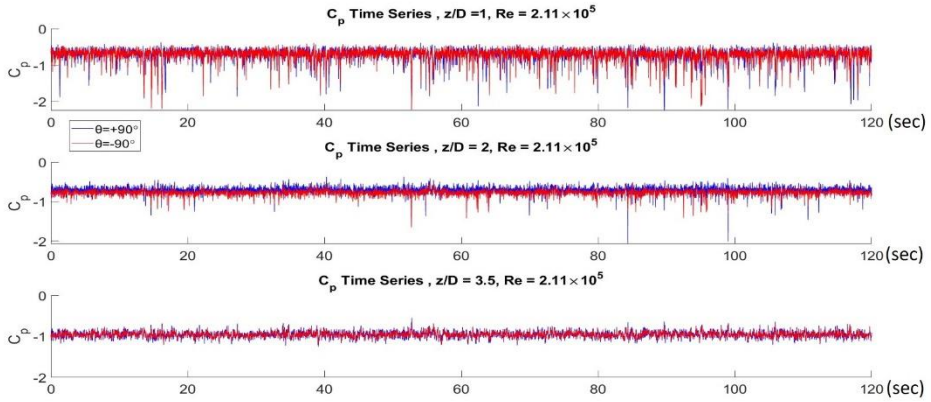

Fig. 6 Comparison of the C_P traces obtained at z/D=1, 2 and 3.5, $\theta = \pm 90°$, at Re= 2.11x10^5. [15]

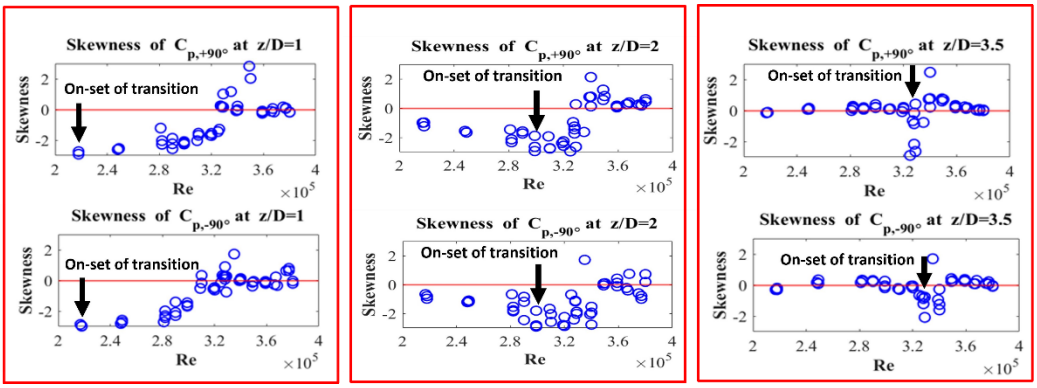

Fig. 7 Variations of the skewness of the C_P traces obtained at z/D=1, 2 and 3.5, $\theta = \pm 90°$ with Re. [15]

4. Concluding remarks

The critical transition ranges identified in the two wind tunnels are found in good agreement, despite that minor discrepancies are noted. The variations of the time-averaged drag and lift coefficient in the critical transition range bear a similarity to those reported in the literature for flow over a two-dimensional circular cylinder. But, the differences between two flows are pointed out subsequently.

In the sub-critical range, flow around the model of the aspect ratio 4 shows the characteristics of the arch-type vortex shedding. On-set of the critical transition is initiated in the base region. In the critical transition range, the horse-shoe vortex in the base region plays the role to damp the unsteadiness of separation bubble formation around the model. Toward the super-critical state, the footprint of the horse shoe vortex in the base region is remarkable.

5. Acknowledgement

Funding support of National Science and Technology Council under the project number NSTC 112-2622-E-006-002-020 is gratefully acknowledged. Acknowledgment should also be made to the previous studies cited in this paper, from which the data are reproduced.

References

[1] Wieselsberger, C., "Further information on the laws of fluid resistance. NACA Technical Notes", TN 121, (1922).

[2] Bearman, P. W., "On vortex shedding from a circular cylinder in the critical Reynolds number regime", *Journal of Fluid Mechanics,* Vol. 37, no. 3, (1969), pp. 577-585.

[3] S. Okamoto and Y. Sunabashiri, "Vortex shedding from a circular cylinder of finite length placed on a ground plane", *Journal of Fluids Engineering,* Vol. 114, no. 4, (1992), pp. 512-521.

[4] Miau, J. J., Chen, Z. L. and Hu, C. C., "The Characteristics of the ABRI wind tunnel", in *Wind Tunnels: Design/Construction, Types and Usage Limitations,* Susan B. Chaplin ed., Nova Science Publishers, New York, (2013), pp. 1-33.

[5] Hsu, X. Y., Miau, J. J., Tsai, J. H., Tsai, Z. X., Lai, Y. H., Ciou, Y. S., Shen, P. T., Chung, P. C. and Wu, C. M., "The aerodynamic roughness of textile materials", *The Journal of the Textile Institute*, Vol. 110, No. 5, (2018), pp. 771-779.

[6] Tsai, J. H., "*Investigations of flow around a finite circular cylinder at critical Reynolds numbers*", Master thesis, Department of Aeronautics and Astronautics, National Cheng Kung University, Tainan, Taiwan, (2018).

[7] Achenbach, E. "Influence of surface roughness on the cross-flow around a circular cylinder", *Journal of Fluid Mechanics,* Vol.46, (1971) pp. 321-335.

[8] Wu, J. C., "*Effect of aspect ratio on the flow around finite circular cylinder in the critical regime*", Master thesis, Department of Aeronautics and Astronautics, National Cheng Kung University, Tainan, Taiwan, (2020).

[9] Tsai, Z. X., "*The design of 2D force balance and the effect of textile roughness on the aerodynamic characteristic of a circular cylinder*", Master thesis, Department of Aeronautics and Astronautics, National Cheng Kung University, Tainan, Taiwan, (2017).

[10] Tsai, M. C., "*Investigations of unsteadiness separation bubble around finite circular cylinder at transition critical regime*", Master thesis, Department of Aeronautics and Astronautics, National Cheng Kung University, Tainan, Taiwan, (2021).

[11] Kawamura, T., Hiwada, M., Hibino, T., Mabuchi, I. and Kumada, M., "Flow around a finite circular cylinder on a flat plate: Cylinder height greater than turbulent boundary layer thickness", *Bulletin of JSME,* Vol. 27, No. 232, (1984), pp. 2142-2151.

[12] Sakamoto, H. and Arie, M. "Vortex shedding from a rectangular prism and a circular cylinder placed vertically in a turbulent boundary layer," *Joural of Fluid Mechanics,* Vol. 126, (1983), pp. 147-165.

[13] Farell, C. and Blessmann, J., "On critical flow around smooth circular cylinders," *Journal of Fluid Mechanics,* Vol. 136, (1983), pp. 375-391.

[14] Schewe, G., "On the force fluctuations acting on a circular cylinder in crossflow from subcritical up to transcritical Reynolds numbers", *Journal of Fluid Mechanics,* Vol. 133, (1983), pp. 265-285.

[15] Zhuang, G. T., "*Effect of aspect ratio on the unsteadiness of separation bubble around finite circular cylinder at transition critical regime*", Master thesis, Department of Aeronautics and Astronautics, National Cheng Kung University, Tainan, Taiwan, (2022).

[16] Humpherys, J. S., "On a circular cylinder in a steady wind at transition Reynolds numbers", *Journal of Fluid Mechanics,* Vol. 9, No. 4, (1960), pp. 603-612.

[17] Lai, Y. H., Miau, J. J., Zhung, G. T., Tsai, M. C., and Wu, J. C., "Characteristics of separation-bubble formation on finite circular cylinder in critical transition range," *AIAA Journal,* Vol. 61, No. 10, (2023), pp. 4468-4484.

[18] Chen, Y. H., Miau, J. J. and Chen Y. R. "Statistical analysis of flow field patterns in critical transition of a finite cylinder using an adaptive threshold method", The 8th International Conference on Jets, Wakes and Separated Flows, ICJWSF-2024, September 23-25, 2024, Firenze, Italy.